Insights into the Impacts of Synthesis Parameters on Lignin-Based Activated Carbon and Its Application for: Methylene Blue Adsorption

Sara Ghane [iD], **Elham Moosavi** [iD], **Ramin Karimzadeh** * [iD]

1. Faculty of Chemical Engineering, Tarbiat Modares University, Tehran, Iran. E-mail: sara.ghane@modares.ac.ir
2. Department of Chemical and Materials Engineering, Buein Zahra Technical University. E-mail: e.moosavi@bzte.ac.ir
3. Faculty of Chemical Engineering, Tarbiat Modares University, Tehran, Iran. E-mail: ramin@modares.ac.ir

ARTICLE INFO	ABSTRACT
	In the current research, lignin was successfully extracted from industrial waste Kraft black liquor using the acid precipitation method. In the following step, powdered carbon was synthesized through the H_3PO_4-chemical activation method. The effects of synthesis parameters, including activation temperature (T) within the range of 400-600 ºC and two H_3PO_4/Lignin mass ratios (R) of 2 and 3 on activated carbon (AC) structure, were investigated. The physical and morphological properties of the ACs were obtained through BET, SEM, and FTIR analyses. The potential application of ACs was studied by measuring their adsorption capacity in the adsorption process of Methylene blue (MB) from an aqueous solution. The sensitized AC at R=2, and T= 500 ºC (AC-2-500) showed the highest specific surface area (1573.31 m^2/g) and the pore volume (0.89 cm^3/g), as well as the highest adsorption capacity of MB. This adsorbent was applied in the equilibrium adsorption experiments and kinetic description. The results from kinetic experiments and adsorption isotherms indicated that the pseudo-first-order model and Langmuir model were in correspondence with the experimental data most. The maximum adsorption capacity was 188 mg/g. The study proved there is a high potential for the conversion of black liquor to greatly porous Lignin-based adsorbents. Moreover, the considerable maximum adsorption capacity suggested a significant potential of Lignin-based AC for wastewater treatment.

Introduction

Water pollution is one of the most severe environmental problems, threatening economic development and human health [1]. As a result of rapid industrialization, waste emissions from many factories, even at low concentrations, cause severe problems for aquatic life and humans [2, 3].

Dyeing, paper and pulp, textiles, plastics, leather, cosmetics, and food industries frequently use dyes to stain products. Their colored effluent contains a wide range of organic compounds and toxic materials [4]. Many of them, including MB can cause irreversible damage to the humans and animals' bodies, such as allergic reactions, a burning sensation in the eyes,

---

vomiting, irritation in skin, or sometimes cancer [5]. Therefore, Several methods have been used to eliminate harmful substances from polluted water, including coagulation [6], electrochemical treatment [7], photocatalysis [8], membrane filtration [9], biological treatment [10], and adsorption [11–13]. Although some processes have received little attention because of their high operating costs, high energy-chemical usage, and poor performance [14,15], adsorption is one of the treatment techniques with high efficiency, selectivity, and easy operation without the production of harmful by-products [16–19]. ACs are well-known adsorbents because of some unique characteristics, including highly developed porosity, great surface area, variable chemistry of the surface, and a high degree of surface reactivity [20,21].

Commercial ACs are expensive adsorbents and the cost of them is highly affected by their quality. Therefore, recent studies have concentrated on producing cost-effective adsorbents, as an alternative for commercial ACs. Different raw materials, such as coal, coconut shells, wood, peat, and various types of lignocellulosic wastes, are used as precursors. Since the chemical activation method mainly produces a much more porous structure compared to the physical activation, it has become widely used in ACs production [22].

Although ACs are still at the center of attention in industries, the development of appropriate manufacturing methods and insights into their porous structure is still ongoing. Accordingly, understanding a way to extend the porosity is necessary, because it contributes to the control and prediction of its performance during applications [23].

Due to rising concerns about energy efficiency and cost-effectiveness, the recovery of biomass waste has been increasingly considered as a bio-source. In recent years, because of the improvements of numerous applications of lignin as a renewable feedstock, the isolation of lignin from black liquor has attracted much attention. Lignin is used as a dispersant, emulsifier, binder, and sequestrant [24]. Lignin, as one of the main constituents of wood and other lignocellulosic materials, is the second most abundant biopolymer on the earth [24]. Lignin molecular structure is a three-dimensional polymer made of phenyl propane units which are randomly linked together [25]. Because of its complexity, the lignin is identified from the presence of phenyl propane units, i.e. p-hydroxyphenyl (or p-coumaryl alcohol), guaiacyl (or coniferyl alcohol), and syringyl (or sinapyl alcohol). As a result, it can be a promising candidate for biomass-based carbon materials, due to its high aromaticity, high thermal stability, and high carbon content [26].

The most significant lignin volume comes from the traditional Kraft pulping process [27]. A liquor containing phenolic compounds is the effluent of the Kraft lignin process. It is dark brown or black, so known as black liquor. Black liquor generally includes toxic chemicals and the derived form of lignin. They must be removed before the effluent is discharged into the environment. In order to reduce the environmental impacts, the pulp and paper industries typically burn the dissolved lignin in the black liquor to generate energy [28]. Powdered lignin can be recovered from black liquor via suitable chemical treatments and filtering processes [26].

Although there have been a number of researches concerning carbonization [29–31] and activation [32, 33] of biomass-based natural resources, studies on the preparation of the ACs from black liquor are still immature. More importantly, most of the previous studies have dealt with the recovery of lignin from lignin-based wastes [24, 34, 35], while in this study we have tried to extract the highest amount of lignin that has the same structure as natural lignin from black liquor. Hence, the present work aims to find an optimum condition for lignin extraction experiments, then, study the feasibility of the production of ACs by H3PO4 activation of lignin, and examine the influence of preparation conditions (activation temperature and H3PO4/lignin mass ratio) on the pore structure of ACs. Moreover, the application of synthesized adsorbents in removing MB, as one of the water pollutants representatives, has been investigated to figure out the relationship between the adsorbent surface and adsorption capacity.

Experimental

Materials

The Kraft Black liquor was supplied by Iran Wood & Paper Industries-Chooka Co. located in the Gilan province of Iran. HCl 37% and H_3PO_4 85% were used to decrease the pH of black liquor and as an activating reagent, respectively. The analytical grade of MB was applied in all adsorption experiments.

Lignin Extraction

The initial measured pH of supplied black liquor was about 10. To extract lignin from black liquor the, HCl 37% was gradually added into three vials containing 100 ml of black liquor, waiting for the pH reached different values of 1, 2, 5. After getting the desired pHs, the solution was stirred at 90 ^{0}C for 1 h. At the end of this step, a visible biphasic solution was obtained. The precipitate was separated through a piece of suction-filtering equipment, washed with distilled water (until neutral pH), dried at 110 ^{0}C for at least 3 h, and finally, ground with a pestle and mortar to obtain lignin powder. The final weight of dry lignin powder was reported to determine production yield.

Activated Carbon Preparation

The extracted lignin was mixed with the activating agent (H_3PO_4 85%) in two ratios of R=2 and 3. Then, the mixture was kept at ambient temperature for 30 minutes to ensure that the activating agent entirely penetrated the lignin pores. This mixture was then dried in the oven at 110 ^{0}C for 24 h to evaporate the water of the H_3PO_4 solution and prepare the impregnated samples. At the end of this step, the mixture converted to a black sticky solid. The samples were thermally treated and heated up to a specific T under continuous N_2 flow at the temperature rate of 10 ^{0}C/min in a tube furnace for 1 h. The T was set at three different points 400, 500, and, 600 ^{0}C. Finally, the activated samples were allowed to be cooled under N_2 flow. To remove the residual H_3PO_4, the samples were washed sequentially many times with hot distilled water until obtaining neutral pH. The resulting ACs were dried at 110^{0}C

Characterization Methods

The surface characteristics of ACs were measured by nitrogen adsorption and desorption method using the device ASAP 2020, Micromeritics at 77 K. Before measuring the adsorption analysis, the samples were outgassed at 250 ^{0}C under vacuum condition for several hours to clean the surface and remove the impurities. The BET method was applied to calculate the BET surface area of ACs, using the adsorption isotherm of nitrogen [34]. The surface chemical properties of extracted lignin at various pHs and prepared ACs were analyzed by Fourier-transformed infrared spectroscopy (FTIR) to determine the existence of different chemical functional groups in the samples applying the KBr pellet method (PerkinElmer device). The surface morphology of extracted lignin and ACs obtained using the means of a field emission scanning electron microscope (FE-SEM; TE-SCAN, MIRAIII). The elemental analysis was determined by EDX analysis applying the previously mentioned device for FE-SEM.

Adsorption Experiments

Since MB has shown strong adsorption on solids, it was chosen as a model compound for adsorption experiments.

To select the best adsorbent among the six synthesized ACs and compare their adsorptive performances, 0.05 g of each prepared AC was added into the 20 ml of MB aqueous solution (initial concentration of 300 ppm and 400 ppm). In the adsorption experiments, one magnet with the appropriate size was placed in the vial containing color solution and ACs to be mixed at room temperature and pressure for 1 hour.

To study adsorption kinetic, the 0.05 g of AC-2-500 sample, which was selected as the most desirable adsorbent, was put into 20 ml of MB aqueous solution (initial concentration of 300 mg/L), and then was shaken at the desired time intervals (10-60 min).

The adsorption isotherms were obtained by immersing the 0.05 g of AC-2-500 sample into 20 ml of MB aqueous solution (300–800 mg/L initial concentrations). In the following step, it was agitated at room temperature until attaining equilibrium.

After reaching the desired times, the ACs were separated from the MB aqueous solution, and the remaining dye concentration was measured using a UV–vis spectrophotometer at 665 nm.

The adsorption capacity of MB onto adsorbent, qt (mg/g) at a certain time(t), and the percent of color removal R(%) of MB were calculated using Eqs. 1 and 2 [35].

$$qt = \frac{(C_0 - C_t) * V}{M} \tag{1}$$

$$R(\%) = \frac{(C_0 - C_t)}{C_0} * 100 \tag{2}$$

where C_0 (mg/L) is the initial concentration of MB; C_t (mg/L) is the residual dye concentration at time(t); V (L) is the volume of dye solution; and M(g) is the mass of adsorbent [35].

Results and Discussion

The Impact of pH Change on the Amount of Extracted Lignin

The effect of pH on the extracted lignin quantity is investigated. The amount of extracted lignin from 100 ml of the supplied black liquor at different pHs is shown in Fig 1.
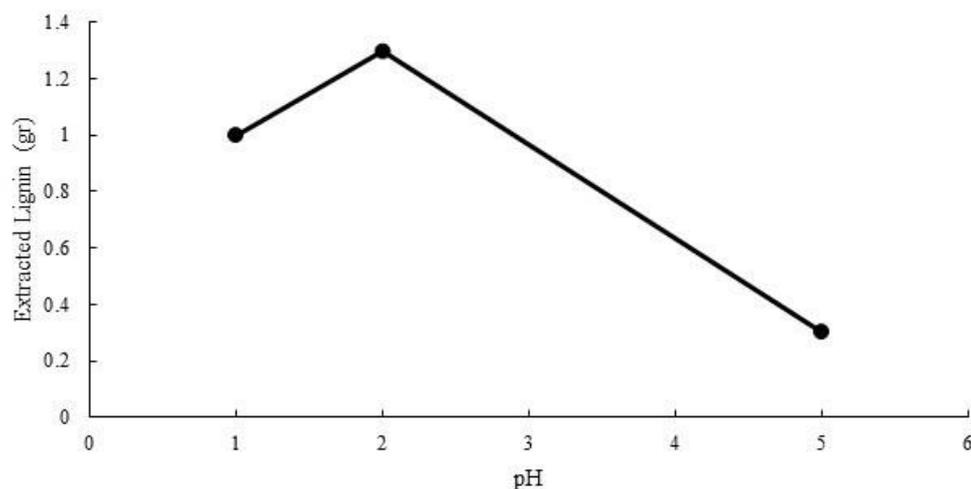
Fig. 1. The weight of extracted lignin at different pHs

It can be concluded from Fig 1, the change in pH has a significant impact on the yield of extracted lignin, and it is optimum at pH=2. In addition, according to Fig 1, it has been found that since an insignificant amount of lignin has been obtained at pH=5 compared to pHs=1 and 2, the extremely acidic environment is necessary to recover lignin from Kraft black liquor. This result is in accordance with Fengel's and Wegener's research [36], which confirms the high solubility of lignin in an alkaline medium. As a result, pH = 2 has been chosen for the next steps to extract lignin from the black liquor as a precursor for the synthesis of ACs.
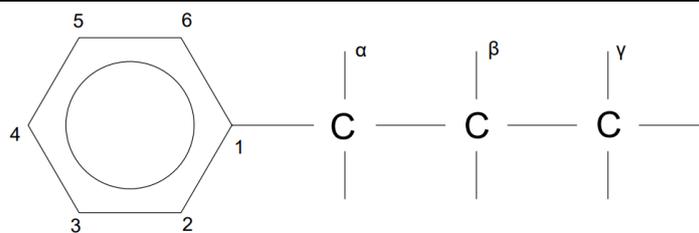
FTIR Analysis

The Impact of pH Change on the Extracted Lignin Chemical Functional Groups

The FTIR spectrum of extracted lignin at different pHs and original black liquor waste on a dry basis is shown in Fig. 2.
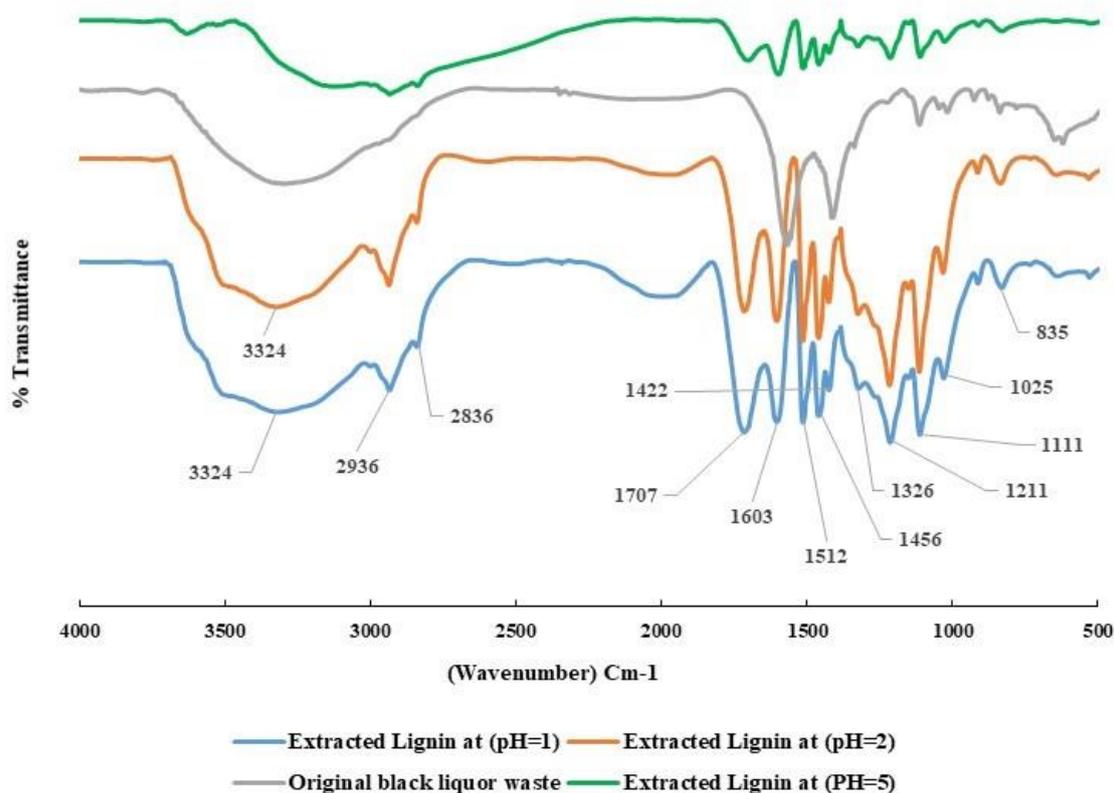
Fig. 2. The impact of pH change on the chemical functional groups of different extracted lignin

According to the FTIR spectroscopy data, the original dried black liquor powder and the different extracted lignin powders have different frameworks. Fig. 2 presents the relatively broad absorption peak at about 3324 cm^{-1}, displaying the existence of hydroxyl groups (OH) in the alcohol and phenol groups in the lignin, which is visible in the precipitations at pHs 1 and 2. The two small peaks observed around 2936 and 2836 cm^{-1} indicate the stretching of C-H from the deformation of methyl and methylene groups [37]. It is confirmed that the peaks around 1707 and 1603 cm^{-1} explain the presence of carbonyl peaks in the β position, and in the α and γ positions of the phenylpropane unit, respectively. It is also observed from the peak around 1025 cm^{-1} the existence of the C-O group owing to the primary alcohol. The presence of peaks around 1512, 1456, and 1422 cm^{-1} can confirm the aromatic ring C=C and 835 cm^{-1} aromatic C-C groups. In addition, the peaks observed at 1326 and 1111 cm^{-1} prove the presence of C-O and C-H groups in the syringyl ring. Furthermore, the observed peaks near 1211 cm^{-1} reveal the C-O and C-H groups in the guaiacyl ring [38]. Hence, the FTIR results prove the successful extraction of lignin from supplied black liquor, especially at pH 1 and 2, because of the similarity of the structure to the natural lignin. Fig. 3 shows the chemical structure of lignin constituents with the base phenylpropane unit [39].

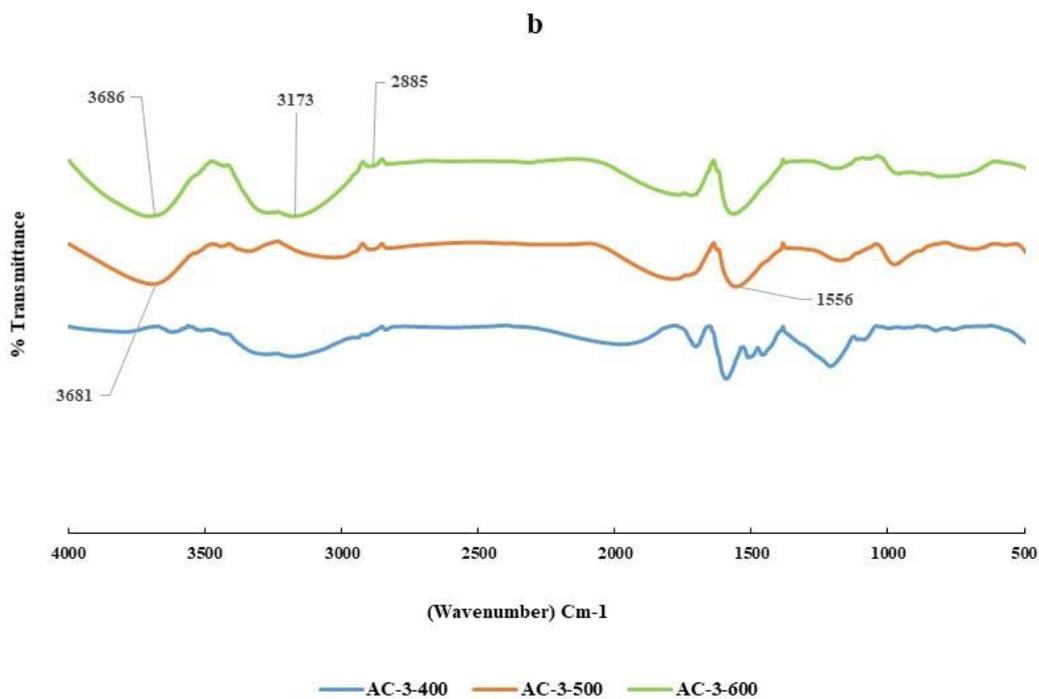**Fig. 3**. Base structure of the phenylpropane unit

FTIR Analysis of Synthesized ACs

The FTIR spectrum of ACs prepared from the extracted lignin at different R=2 and 3 based on the temperature change are shown in Fig. 4.

b
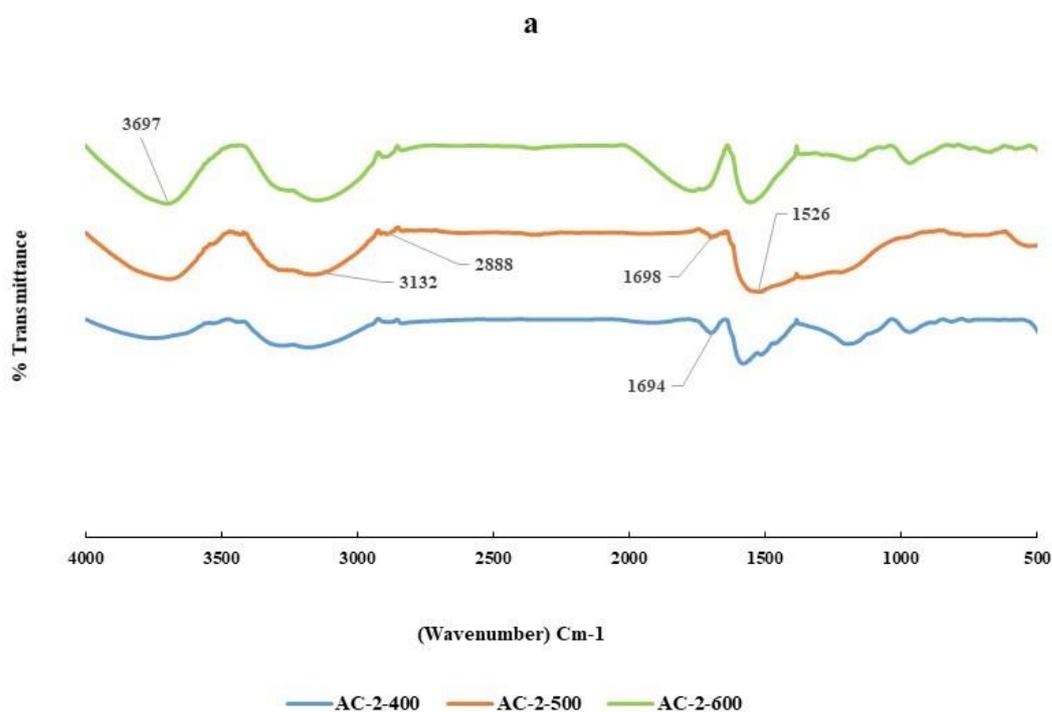
Fig. 4. FTIR analysis spectrum of ACs (R=2 (a) and 3 (b))

According to Fig. 4, it is clear that the intensity of peaks decreases after the activation process compared to the peaks obtained from Fig. 2, indicating that the higher content of the relevant functional groups present in the raw lignin because of its complex nature. All ACs display a broad peak in the range (3700-3680) cm^{-1} that is referred to as the O-H stretching vibration of the hydroxyl group. The observed bands at (3200-3100) cm^{-1} & (2890-2880) cm^{-1} result from the C-H stretching vibration of methyl and methylene groups. The band at (1700-1690) cm^{-1} is related to the C=O stretching vibration. The band around (1560-1520) cm^{-1} ascribes to aromatic ring stretching vibration [40, 41].
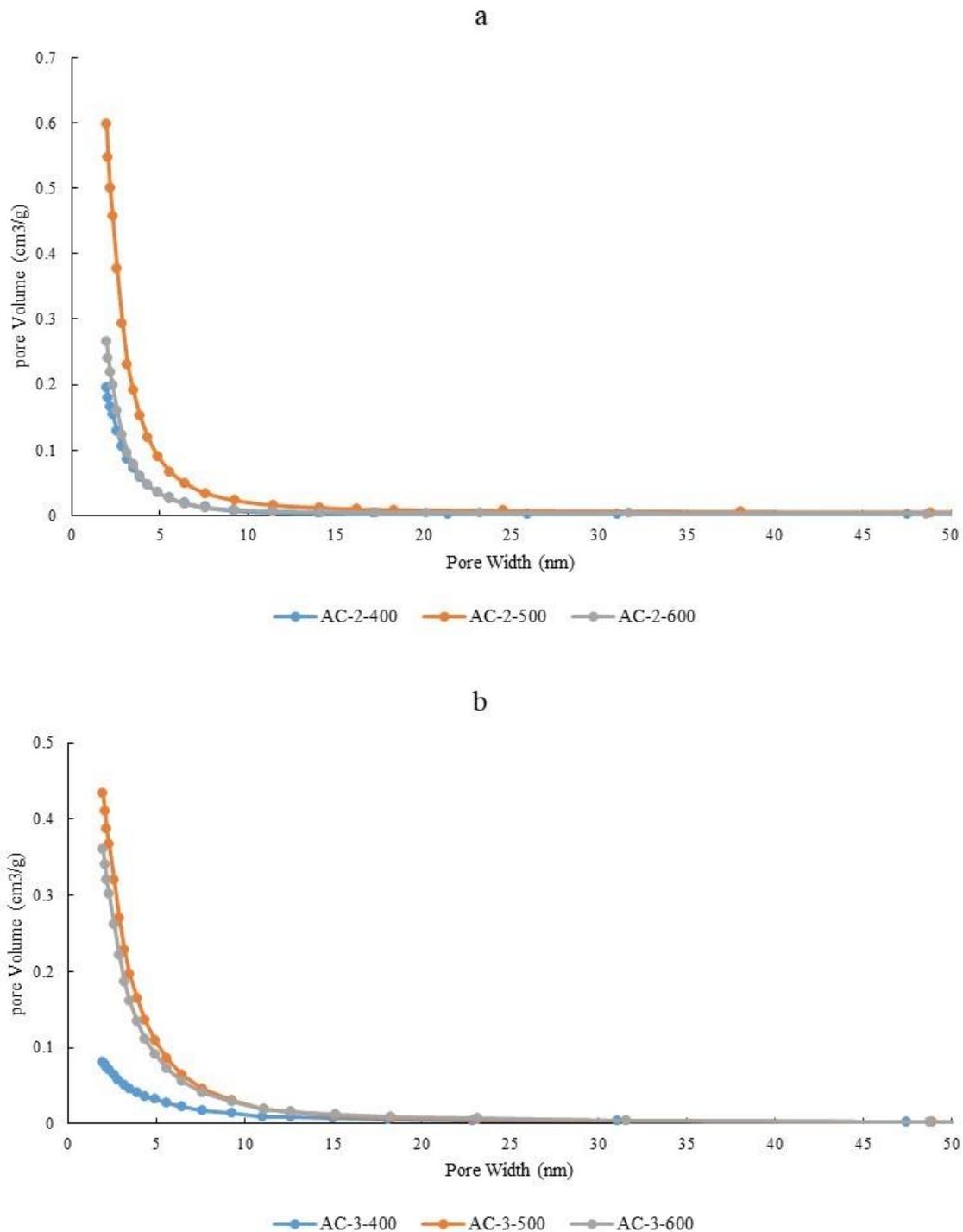
BET Analysis

Fig. 5 presents the nitrogen adsorption/desorption curves of the ACs prepared at R= 2 and 3 based on the temperature change.
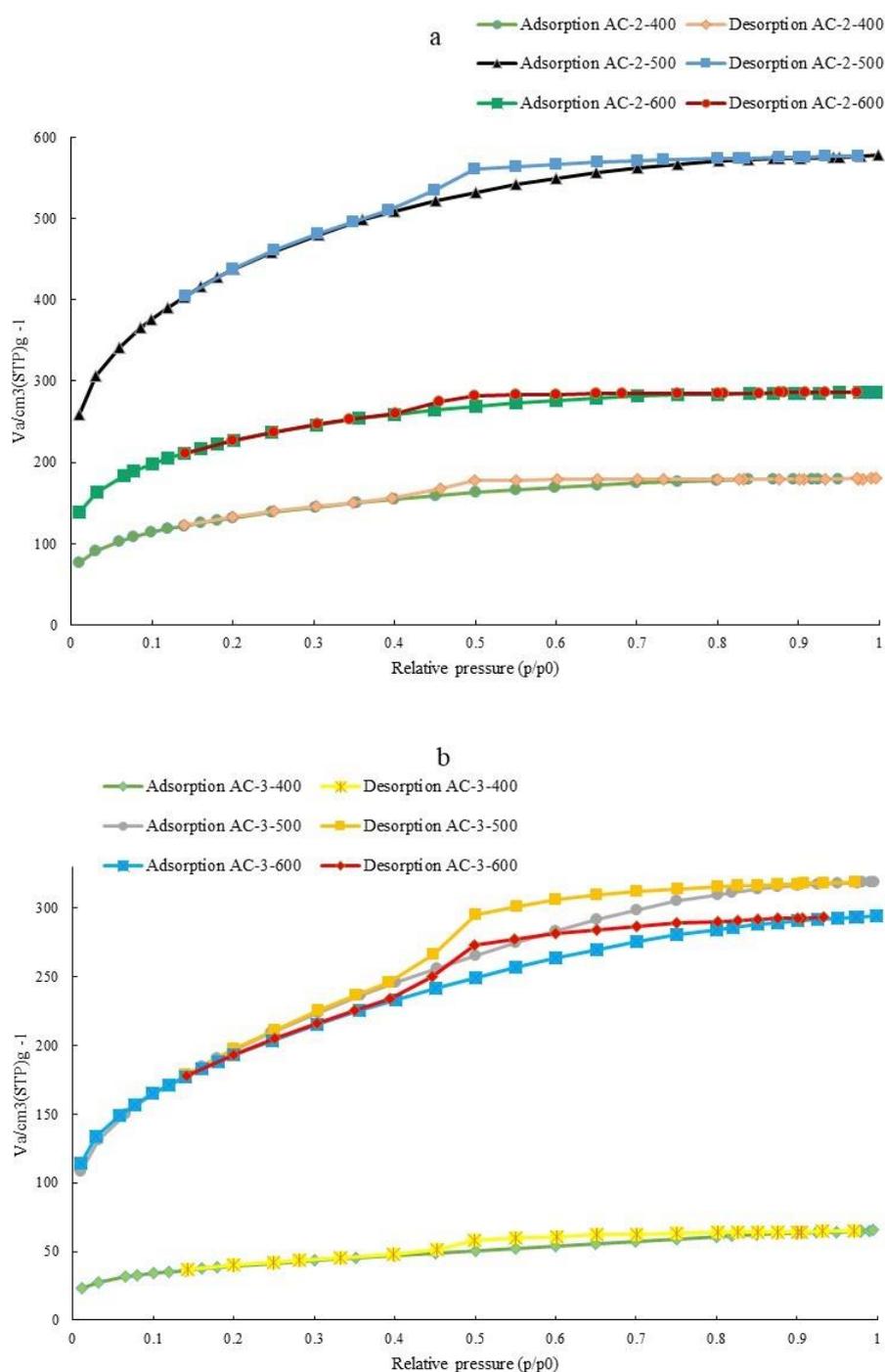
Fig. 5. Nitrogen adsorption/desorption curves of ACs (R= 2 (a) and 3 (b))

From Fig. 5, it can be concluded that all ACs follow the type I isotherm, which is a reflection of a predominantly microporous structure with a mesoporosity contribution. It should be noted that type I isotherms also are applicable for the adsorbents which include very small mesopores (close to micropores (0-2 nm)) [42]. This result is consistent with the average pore diameter in Table 1 (Dp are in the range of ~ 2.17 to 2.82). In other words, the majority of pores are located in the mesopore region that are very close to micropores in size. Additionally, the formation of some hysteresis around the relative pressure of 0.5 proves the existence of mesopores in the adsorbents. Moreover, 2 samples of AC-2-400 and AC-3-400 are expected to have a small surface area and pore volume compared to the other samples due to their lower amount of N_2 adsorption.

The distribution of pore size of ACs in different R= 2 and 3, obtained from the BJH diagram, are illustrated in Fig. 6. As seen, the distribution of pore size for all ACs is mainly located in the range of 2-5 nm.

a

b

Fig. 6. The distribution of pore size of ACs (R= of 2 (a) and 3 (b))

Table 1 gives information about the structural characteristics of synthesized ACs. Additionally, the effects of change in T and R on the BET surface area are shown in Fig. 7.

Table 1. BET analysis' results

Samples	S_{BET} (m^2/g)	S_{micro} (m^2/g)	S_{meso} (m^2/g)	V_{tot} (cm^3/g)	V_{micro} (cm^3/g)	V_{meso} (cm^3/g)	D_p (nm)
AC-2-400	474.6712	90.1438	384.5273	0.2779	0.035	0.2429	**2.3423**
AC-2-500	1573.3173	268.1397	1305.1776	0.8910	0.1039	0.7871	**2.2655**
AC-2-600	812.6715	209.9339	602.7376	0.4421	0.0868	0.3553	**2.1765**
AC-3-400	141.7149	22.8058	118.9091	0.1001	0.0088	0.0913	**2.8271**
AC-3-500	720.3628	16.8112	703.5515	0.4922	0.0350	0.4572	**2.7333**
AC-3-600	696.2931	91.4802	604.8129	0.4533	0.0334	0.4199	**2.6045**
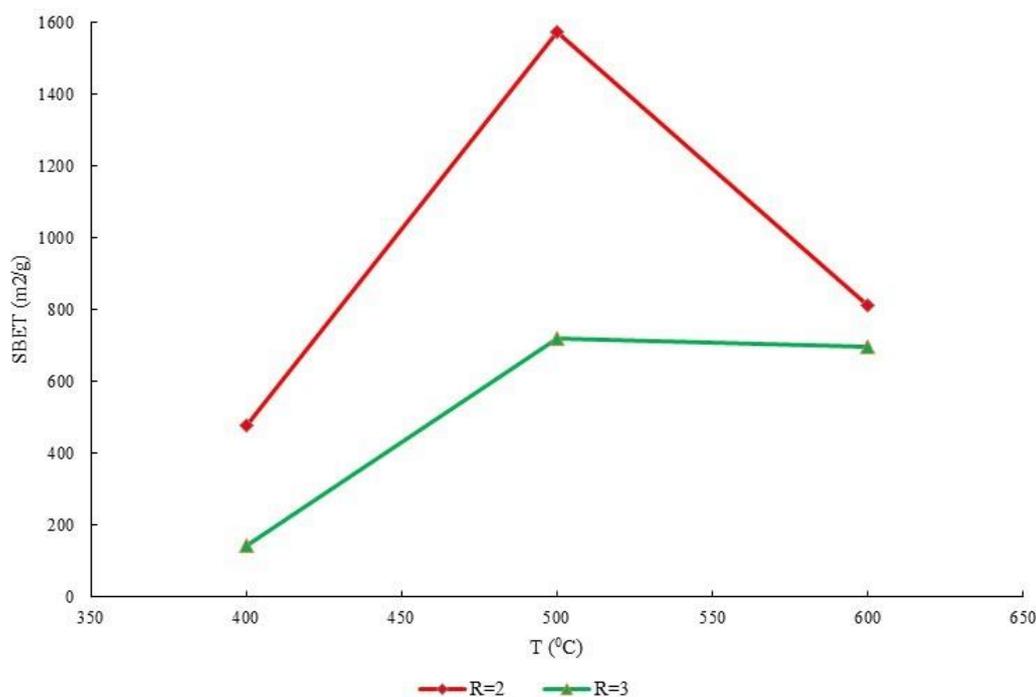
Fig. 7. Effects of change in T and R on the BET surface area

It is observed that as T increases (in both R= 2 and 3) from 400 to 500 ^{0}C, BET surface area significantly enhances as well, and then decreases with a further increase up to 600 ^{0}C. Similarly, the pore volume reduces, probably because of heat shrinkage of the carbon structure. In contrast, at a constant temperature and increasing the R, BET surface area decreases. As a result, raising the temperature above 500 ^{0}C and R from 2 to 3 does not have a positive impact on BET surface area. It could be anticipated that as long as H_3PO_4 can react with lignin, an increment within the volume filled by phosphate and polyphosphate compounds will occur. However, the carbon structure may likely be weakened by the attack of an excess amount of acid. Hence, there is an optimum amount of acid that can react with lignin; the higher R leads to extensive breakage of biopolymer bonds, shrinkage of the structure, and finally, a reduction in surface area and, to a similar extent, total pore volume [43]. As it is shown in Table 1, the R can also affect the distribution of porosity. The average figure of V_{meso} to V_{tot} is ~85% in the ACs at R=2, while this reached ~92% at R=3. Similarly, the presence of more mesopores can be confirmed by comparing the pore diameters from R=2 to 3. Therefore, using a higher R leads to a broadening of the porous structure of ACs with a higher contribution of mesopores to the total porosity, but it decreases the surface areas. This result agrees with studies reported by other authors using H_3PO_4 to activate lignin from Kraft black liquor [43, 44].

Considering the above-mentioned results, an AC sample with a maximum BET surface area of 1573.3173 m^2/g and total pore volume of 0.8910 cm^3/g is prepared at T=500 ^{0}C and R=2 (AC-2-500 sample), verifying that H_3PO_4 works as an effective activating agent to produce a

well-developed AC from lignin of black liquor. Many studies have investigated the production of ACs with H_3PO_4 activation of Kraft lignin as a precursor. In the earlier studies, the maximum BET surface areas reached 1459 m^2/g at T=425 ^{0}C and R=2 [44], 1305 m^2/g at T= 600 ^{0}C and R=1.4 [43], and 1972 m^2/g at T=700 ^{0}C and R=7 [45], which are pretty close to our results. Although relatively high BET surface areas have already been reported, in the current study, a high BET surface area has been obtained in a moderate value of T and R. This contributes to less consumption of energy and chemical in carbonization and activation steps.

Table 2 shows the elemental analysis of the raw extracted lignin, AC-2-500, and AC-3-400, which present the highest and lowest BET surface area, respectively.

Table 2. Elemental analysis results

Elements (wt%)	C	N	O	P	S
Lignin	57.42	12.82	26.10	0.16	3.49
AC-2-500	60.83	23.10	13.11	2.08	0.87
AC-3-400	48.41	11.50	33.49	5.11	1.49

The residual P content on the AC-2-500's surface is 2.08 wt%, whereas this figure reaches 5.11 wt% on the AC-3-400's surface. In contrast, C content decreases from 60.83 wt% to 48.41 wt% in AC-3-400. It can be concluded that the weakening of carbon structure takes place by the excess amount of H_3PO_4.

In total, the higher P content in the two mentioned ACs compared to the raw extracted lignin can prove that the H_3PO_4 plays an influential role in surface activation.

FESEM Analysis

Fig. 8 represents FESEM images (magnifications 10 µm and 200 nm) observed from the surface of raw extracted lignin and the sample AC-2-500, which has presented the highest BET surface area.
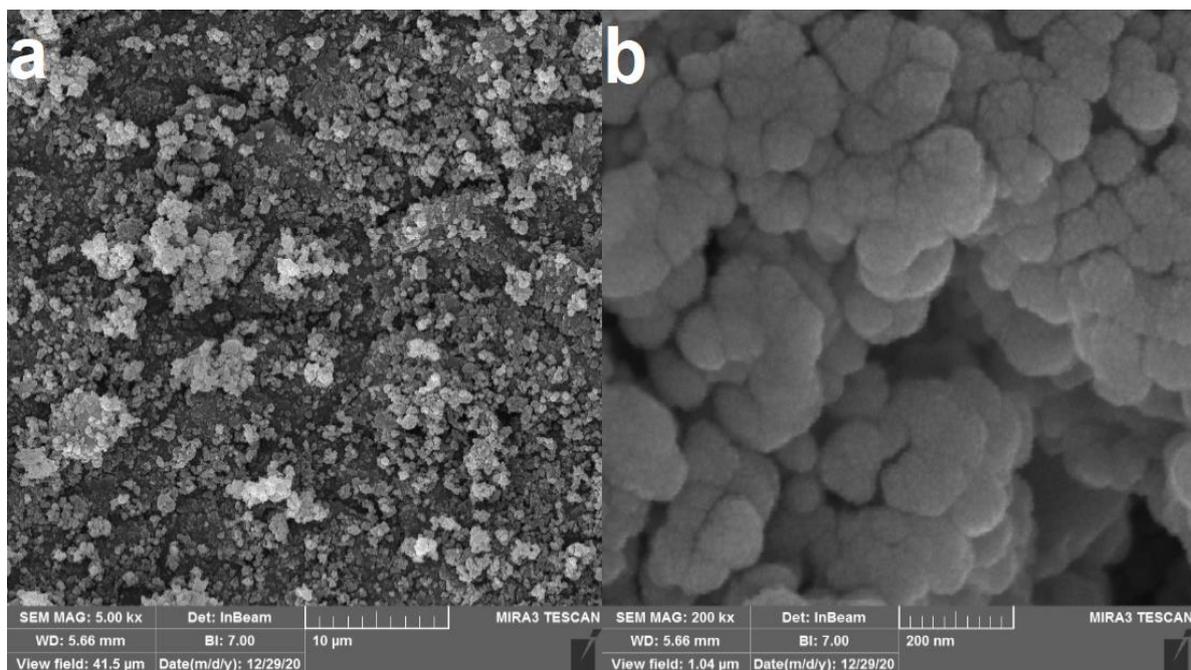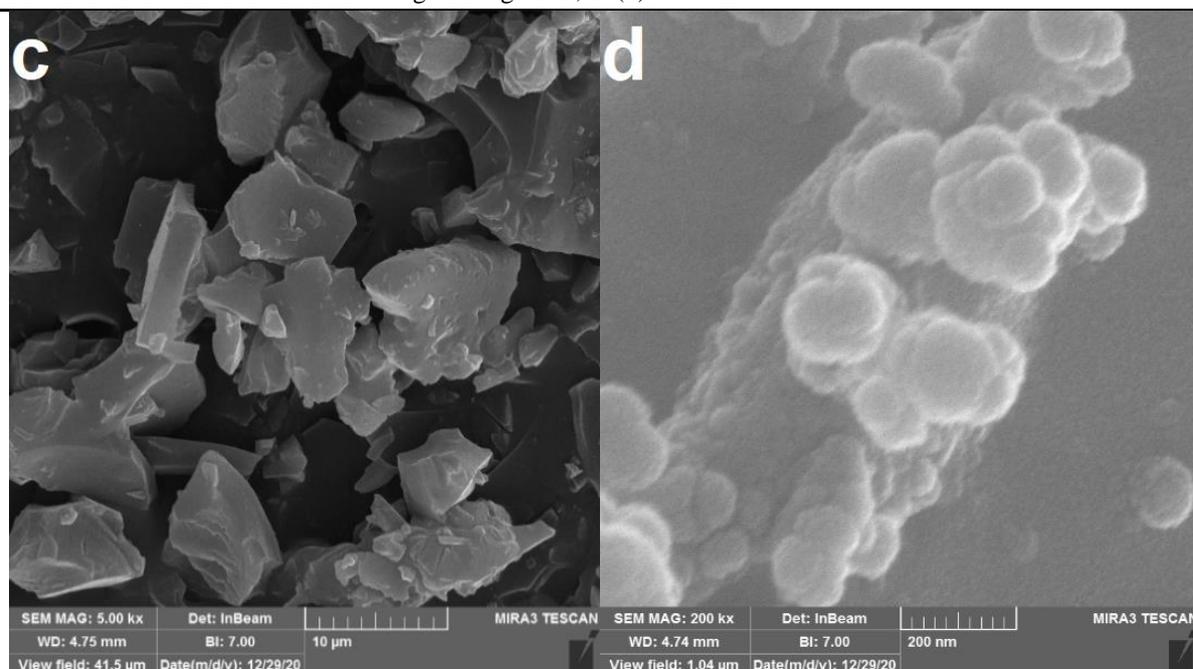
Fig. 8. FESEM images of raw extracted lignin (a, b) and AC-2-500 (c, d)

Lignin as raw material presents few pores before the activation and carbonization processes, because of the presence of volatile gases, and other compounds. However, after that, the structure changes differently. To elaborate, as a result of the lignin reaction with the H_3PO_4, a large number of various sizes and shapes of pores appear on the surface of AC-2-500. This confirms that H_3PO_4 activating agent is effective in forming pores in the raw precursor.

Methylene Blue Adsorption

Selection of the Best Adsorbent

The samples, AC-2-400 and AC-3-40, gave a poor performance in the adsorption of MB, and the intensity of the remained color was much more than the other samples. So, in the next step, the concentration of the residual MB in the other four samples was measured. Table 3 and Table 4 give information about the results of the adsorption experiments.

Table 3. Results of adsorption ability of synthesized ACs (initial MB concentration of 300 ppm)

Samples	Remained MB concentration after adsorption (ppm)	(mg/g)Adsorption capacity	Percentage of MB removal (%)
AC-2-500	0.47	119.812	**99.84**
AC-3-500	0.66	119.736	**99.78**
AC-2-600	0.77	119.692	**99.74**
AC-3-600	0.73	119.708	**99.75**

Table 4. Results of adsorption ability of synthesized ACs (initial MB concentration of 400 ppm)

Samples	Remained MB concentration after adsorption (ppm)	(mg/g)Adsorption capacity	Percentage of MB removal (%)
AC-2-500	0.95	159.62	**99.76**
AC-3-500	7.77	156.892	**98.05**
AC-2-600	37.51	144.996	**90.62**
AC-3-600	12.98	154.808	**96.75**

The AC-2-500 has shown the highest adsorption capacity and the percentage of MB removal from the aqueous solution, from Table 3 and Table 4. In Fig. 9, the qualitative results of adsorption experiments carried out at an initial MB concentration of 400 ppm, can be seen.
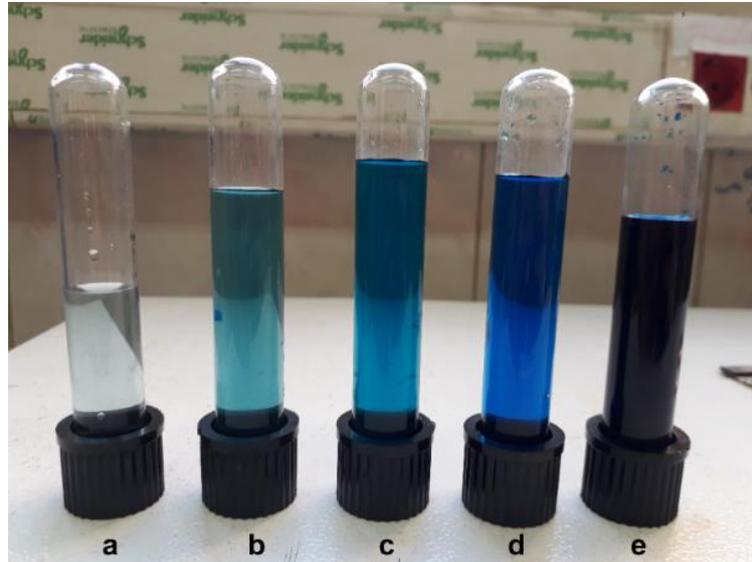
Fig. 9. Qualitative amount of remaining MB after the adsorption process at a concentration of 400 ppm (Based on the lowest remaining MB concentration, i.e., the highest absorption capacity of absorbent, a: AC-2-500, b: AC-3-500, c: AC-3-600, d: AC-2-600, e: MB sample (400 ppm) before adsorption process)

According to the color of the samples, the AC-2-500 sample has presented the highest adsorption capacity and color removal percentage, enabling to adsorb ~100% of the color. As previously explained in part 3.3, the mentioned sample has demonstrated the maximum BET surface area as well. Besides, there is a direct relationship between mesopores' surface area and pore volume and the adsorption capacity of synthesized adsorbents. In other words, the higher surface area, and pore volume in the mesopore region contribute to the greater adsorption capacity of the adsorbent.

Therefore, AC-2-500, as the sample with maximum BET surface area, the highest amount of pore volume, and surface area in the mesopore region is chosen as the best-synthesized sample in the optimum conditions of T=500 ^{0}C and R=2. Further, kinetics and equilibrium adsorption experiments will be carried out on this sample.

Adsorption Isotherms

In adsorption studies, the isotherms are applied to explain the interaction between the adsorbent and adsorbate. In the current study, two famous isotherms, Langmuir and Freundlich, are fitted to the experimental data by the non-linear curve fitting method in order to obtain a proper model for explaining the adsorption of MB onto AC-2-500.

The Langmuir isotherm is defined based on two important assumptions: 1) Adsorption happens on the homogeneous sites of the adsorbent surface, and 2) it refers to monolayer adsorption [46]. The Langmuir Eq. is expressed as follows:

$$q_e = K_L \frac{q_{max} C_e}{(1 + K_L C_e)} \tag{3}$$

q_e (mg/g), C_e (mg/L), K_L (L/mg), and q_{max} (mg/g) define the amount of adsorption at equilibrium, the concentration of MB in the equilibrium state, Langmuir constant, and the maximum monolayer adsorption capacity, respectively [35]. The Langmuir isotherm constant can be expressed as a dimensionless parameter known as the separation factor (R_L) [47], defined by Eq. 4:

$$R_L = \frac{1}{1 + K_L C_0} \tag{4}$$

where R_L refers to how much the adsorption process is favorable; It is favorable when $0 < R_L < 1$, unfavorable when $R_L > 1$, linear when $R_L = 1$, or irreversible when $R_L = 0$ [47].

By contrast, the Freundlich isotherm is based on the heterogeneous surface of the adsorbent and is employed for the multilayer adsorption process. The following Equation describes the Freundlich isotherm [48]:

$$q_e = K_F C_e^{\frac{1}{n}} \tag{5}$$

K_F (mg/g (L/mg)$^{1/n}$) is the Freundlich isotherm constant, related to the adsorption capacity of the adsorbent, and $1/n$ ranges between 0 and 1 is a measure of the Freundlich adsorption intensity parameter or surface heterogeneity, becoming more heterogeneous as its value approaches zero. When the value of $1/n$ stay below unity presents a normal Langmuir isotherm, while $1/n$ above unity shows cooperative adsorption [49].

In Fig. 10, the Langmuir and Freundlich adsorption isotherms are fitted to experimental data.
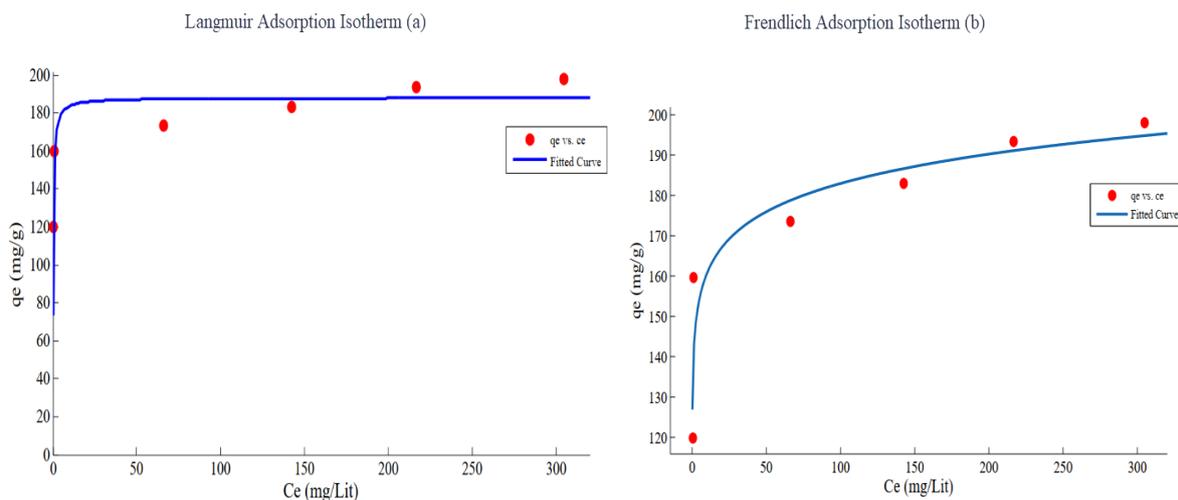
Fig. 10. Adsorption isotherms of MB onto AC-2-500

The calculated constants from Langmuir and Freundlich adsorption isotherms and correlation coefficient (R^2) are summarized in

The R^2 derived from the Langmuir and Freundlich equations are 0.8894 and 0.8422, confirming that both isotherms are well-fitted with the equilibrium data. However, the greater R^2 from Langmuir isotherm compared to Freundlich isotherm confirms that Langmuir isotherm is a more reliable equation in modeling and describing the adsorption behavior of the MB-AC system. The obtained results also reveal that the homogenous nature of the surface of the adsorbent and monolayer adsorption have taken place on the surface of AC-2-500. Additionally, the maximum monolayer adsorption capacity calculated from Langmuir isotherm reaches 188 mg/g, suggesting that the adsorption capacity of AC-2-500 in the removal of dye from aqueous solution is relatively high. This can be proved by comparing different adsorbents' capacities reported in the recent research (see Table 7). R_L parameter is calculated for all initial

MB concentrations and varies within the range of 0-1 and verifies that the synthesized AC-2-500 is favorable for MB adsorption under the applied condition. As is also mentioned in the value of 1/n=0.056 is less than 1, which means the adsorption is favorable.

Table 5. Constants of Langmuir and Freundlich adsorption isotherms for MB removal by AC-2-500

Langmuir isotherm	
q_{max} (mg/g)	188
K_L	4.295
R_L	$2.9*10^{-4}$-$7.7*10^{-4}$
R^2	0.8894
Freundlich isotherm	
K_F	141.1
1/n	0.056
R^2	0.8422

Adsorption Kinetics

To study the rate and the mechanism of the adsorption kinetic, three kinetic models are introduced by the non-linear curve fitting method; the Pseudo-first-order model (PFO), the pseudo-second-order model (PSO), and the intraparticle diffusion model [50].

PFO (Eq. 6) and PSO (Eq. 7) are plotted to fit the experimental data, and their equations are presented below:

$$q_t = q_e(1 - e^{-k_1 t}) \tag{6}$$

$$q_t = \frac{K_2 q_e^2 t}{1 + K_2 q_e t} \tag{7}$$

where k_1 (1/min) and K_2 (g/mg.min) are the rates constant of PFO and PSO adsorption, and t (min) is the adsorption time [50].

The PFO and PSO models cannot determine the diffusion mechanism and only describe the sorption behavior over the whole adsorption process. Therefore, further investigation is conducted to identify the mechanism of adsorption using Weber-Morris intraparticle diffusion model defined by the following equation:

$$q_t = K_{id} t^{1/2} + C \tag{8}$$

K_{id} (mg/g.min$^{0.5}$) is the intraparticle diffusion rate constant, and the intercept of C is related to the boundary layer effect [51].

Fig. 11 displays the non-linear graphs of PFO, PSO, and intraparticle diffusion models, respectively.
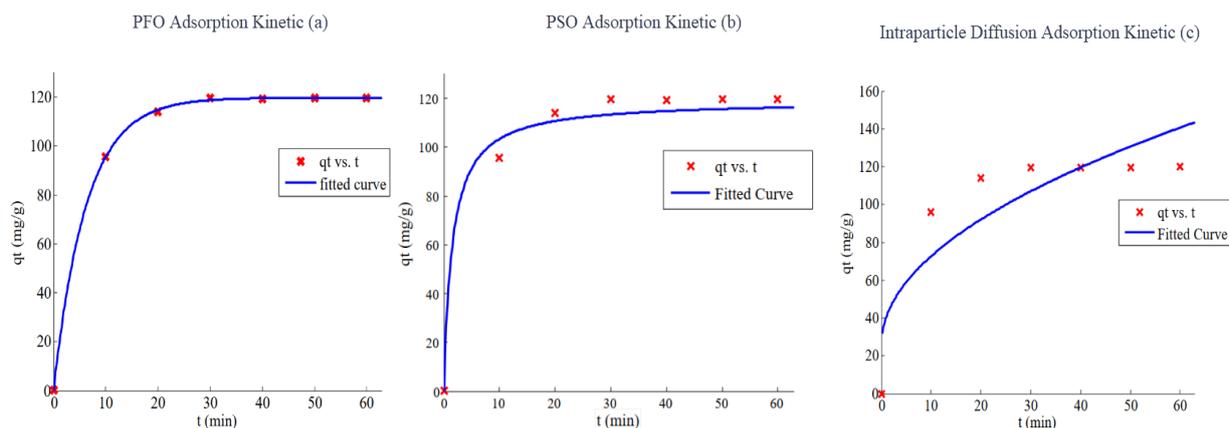
Fig. 11. Kinetic models for the adsorption of MB onto AC-2-500

The kinetic constants and the correlation coefficient (R^2) from these three models are evaluated and presented in Table 6.

Table 6. Kinetic constants for the adsorption of MB onto AC-2-500

PFO	
K_1 (1/min)	0.1598
$q_{e, cal}$ (mg/g)	119.8
$q_{e, exp}$ (mg/g)	119.656
R^2	0.9999
PSO	
K_2 (g/mg.min)	0.0054
$q_{e, cal}$ (mg/g)	119.2
$q_{e, exp}$ (mg/g)	119.656
R^2	0.9867
Intraparticle diffusion	
K_{id} (mg/g min$^{0.5}$)	14.84
C	25.69
R^2	0.7959

As is seen in kinetic ($q_t - t$) graphs, the ability of the adsorbent in the adsorption of MB increases with time. Adsorption kinetic on the adsorbent surface is almost fast. So, the adsorbent can quickly adsorb the MB in the first 30 minutes. Then, the kinetic of MB adsorption ultimately decreases to reach an equilibrium when no significant change in the amount of adsorbed MB can be seen. The reason is that in the initial time of the adsorption process, there is a high volume of unoccupied active sites, but after a while, most of the active sites react with absorbent. As a result, the kinetic of the adsorption process declines. In other words, this speed reduction results from the decrement in the total surface area of the adsorbent during the adsorption process.

Comparison of the correlation coefficients suggests that the PFO kinetic model with the value of $R^2 = 0.9999$ is in high accordance with experimental data, implying the applicability of the PFO equation and the first-order nature of the adsorption process onto AC-2-500. Moreover, R^2 data resulting from the intraparticle diffusion kinetic model is obtained at 0.7959, which is in less agreement with the experimental data compared to the two other models. According to this model, when C is not zero, it confirms that there is an initial resistant boundary layer, and a greater C, revealing more effectiveness of the boundary layer. In addition, the presence of C ensures that intraparticle diffusion is not the only affecting factor on the rate-controlling step, and other kinetic models and various processes can also contribute to the adsorption process.

From Fig. 11c, the graph can be considered as three different lines, suggesting three different stages during the adsorption process. The first stage, the fastest one, is completed in the first 10 minutes and can be attributed to the mass transfer of MB from the solution onto the external surface of the adsorbent. The second stage which takes place in 10-30 minutes, describes the gradual absorption on which intraparticle diffusion is the rate-limiting. At the final stage, intraparticle diffusion decreases to reach an equilibrium.

Table 7 compares various adsorbents in terms of their capacity and kinetic nature for the adsorption of MB, which is found in some recent literature.

Table 7. Comparison of different adsorbents' capacity and kinetic nature

Adsorbents	Maximum adsorption capacity (mg/g)	Isotherm	Kinetic	References
Lignin-based activated carbon	188	Langmuir	PFO	This study
Sisal-activated carbon/cellulose biocomposite film	103.7	Langmuir	PSO	[37]
Polyamide modified -Vermiculite Nanocomposite	76.42	Langmuir	PSO	[52]
Magnetic adsorbent derived from corncob	163.93	Langmuir	PSO	[53]
Biomass adsorbent from Chemically treated date stones	515.46	Langmuir	PSO	[54]
Conventional ZSM-5 zeolite (CZ)	105.82	Langmuir	PSO	[55]
Nanosheet MFI zeolite (NZ)	476.19	Langmuir	PSO	[55]

Conclusions

In the current research, lignin was successfully recovered from waste Kraft black liquor using acid precipitation. The activation of extracted lignin was carried out through the H_3PO_4 chemical activation method to prepare biomass-based ACs. The results showed that the changes in pH of the black liquor has a significant impact on the yield of extracted lignin, and this was optimum at pH=2. The results from FTIR analysis confirmed the successful extraction of lignin from the supplied black liquor. The AC-2-500 sample presented the maximum BET surface area of 1573.3173 m2/g and total pore volume of 0.8910 cm3/g, confirming the effectiveness of H_3PO_4 chemical agent, and the great potential of the supplied black liquor to a well-developed pore structure AC. As the T increased, the BET surface area and pore volume significantly increased over the range of 400 to 500 0C, then, it decreased with a further increment in temperature up to 600 0C, suggesting that increasing the temperature above 500 0C is not effective, probably due to the heat shrinkage of carbons structure. Moreover, by increasing the R from 2 to 3, BET surface area and total pore volume decreased, possibly because of ACs structure weakened by the attack of excess H_3PO_4. By contrast, the use of a higher R led to a greater contribution of mesopores to the total porosity. The kinetic study of MB onto AC-2-500 revealed that the adsorption of MB was fast, and the adsorption kinetic and equilibrium data can be best described by the PFO model, and Langmuir isotherm, respectively. Additionally, the maximum monolayer adsorption capacity calculated from Langmuir isotherm

reached 188 mg/g, suggesting the nearly high adsorption capacity of AC-2-500 for the MB removal.

Nomenclature

AC	Activated carbon
C	Boundary layer effect
C_0	Initial MB concentration (mg/L)
C_e	MB concentration at equilibrium (mg/L)
C_t	Residual MB concentration at time t (mg/L)
K_1	Pseudo-first-order model constant (1/min)
K_2	Pseudo-second-order model constant (g/mg.min)
K_F	Freundlich constant (mg/g (L/mg)$^{1/n}$)
K_{id}	Intraparticle diffusion constant (mg/g.min$^{0.5}$)
K_L	Langmuir constant (L/mg)
M	Adsorbent mass (g)
MB	Methylene blue
n	Freundlich adsorption intensity parameter
PFO	Pseudo-first-order model
PSO	Pseudo-second-order model
q_e	Adsorption capacity at equilibrium (mg/g)
q_{max}	Maximum adsorption capacity (mg/g)
q_t	Adsorption capacity at time t (mg/g)
R	H_3PO_4/Lignin mass ratio
R%	Color removal percentage
R^2	Correlation coefficient
T	Activation temperature (^0C)
t	Adsorption time (min)
V	The volume of dye solution (L)

References

[1]   Saravanan R, Khan MM, Gupta VK, Mosquera E, Gracia F, Narayanan V, et al. ZnO/Ag/CdO nanocomposite for visible light-induced photocatalytic degradation of industrial textile effluents. J Colloid Interface Sci. 2015; 452:126–33. https://doi.org/10.1016/j.jcis.2015.04.035

[2]   Saravanan R, Karthikeyan N, Gupta VK, Thirumal E, Thangadurai P, Narayanan V, et al. ZnO/Ag nanocomposite: an efficient catalyst for degradation studies of textile effluents under visible light. Mater Sci Eng C. 2013;33(4):2235–44. https://doi.org/10.1016/j.msec.2013.01.046

[3]   Saravanan R, Karthikeyan S, Gupta VK, Sekaran G, Narayanan V, Stephen A. Enhanced photocatalytic activity of ZnO/CuO nanocomposite for the degradation of textile dye on visible light illumination. Mater Sci Eng C. 2013;33(1):91–8. https://doi.org/10.1016/j.msec.2012.08.011

[4]   Ramakrishna KR, Viraraghavan T. Dye removal using low-cost adsorbents. Water Sci Technol. 1997;36(2–3):189–96. https://doi.org/10.1016/S0273-1223(97)00387-9

[5]   Ghosh D, Bhattacharyya KG. Adsorption of methylene blue on kaolinite. Appl Clay Sci. 2002;20(6):295–300. https://doi.org/10.1016/S0169-1317(01)00081-3

[6]   Ali I, Asim M, Khan TA. Arsenite removal from water by electro-coagulation on zinc–zinc and copper–copper electrodes. Int J Environ Sci Technol. 2013;10(2):377–84. https://doi.org/10.1007/s13762-012-0113-z

[7]   Ghimire U, Jang M, Jung SP, Park D, Park SJ, Yu H, et al. Electrochemical removal of ammonium nitrogen and cod of domestic wastewater using platinum coated titanium as an anode electrode. Energies. 2019;12(5):883. https://doi.org/10.3390/en12050883

[8]   Saravanan R, Sacari E, Gracia F, Khan MM, Mosquera E, Gupta VK. Conducting PANI stimulated ZnO system for visible light photocatalytic degradation of coloured dyes. J Mol Liq. 2016; 221:1029–33. https://doi.org/10.1016/j.molliq.2016.06.074

[9]   Saleh TA, Gupta VK. Synthesis and characterization of alumina nano-particles polyamide membrane with enhanced flux rejection performance. Sep Purif Technol. 2012; 89:245–51. https://doi.org/10.1016/j.seppur.2012.01.039

[10]   Klauck CR, Rodrigues MAS, Silva LB. Evaluation of phytotoxicity of municipal landfill leachate before and after biological treatment. Brazilian J Biol. 2015; 75:57–62. https://doi.org/10.1590/1519-6984.1813

[11]   Huang Z, Li Y, Chen W, Shi J, Zhang N, Wang X, et al. Modified bentonite adsorption of organic pollutants of dye wastewater. Mater Chem Phys. 2017; 202:266–76. https://doi.org/10.1016/j.matchemphys.2017.09.028

[12]   Gupta VK, Nayak A, Agarwal S, Tyagi I. Potential of activated carbon from waste rubber tire for the adsorption of phenolics: effect of pre-treatment conditions. J Colloid Interface Sci. 2014; 417:420–30. https://doi.org/10.1016/j.jcis.2013.11.067

[13]   Saravanan R, Gupta VK, Narayanan V, Stephen A. Visible light degradation of textile effluent using novel catalyst ZnO/γ-Mn2O3. J Taiwan Inst Chem Eng. 2014;45(4):1910–7. https://doi.org/10.1016/j.jtice.2013.12.021

[14]   Ahmadi M, Niari MH, Kakavandi B. Development of maghemite nanoparticles supported on cross-linked chitosan (γ-Fe2O3@ CS) as a recoverable mesoporous magnetic composite for effective heavy metals removal. J Mol Liq. 2017; 248:184–96. https://doi.org/10.1016/j.molliq.2017.10.014

[15]   Kermani M, Izanloo H, Kalantary RR, Barzaki HS, Kakavandi B. Study of the performances of low-cost adsorbents extracted from Rosa damascena in aqueous solutions decolorization. Desalin Water Treat. 2017; 80:357–69. https://doi.org/10.5004/dwt.2017.21019

[16]   Tan IAW, Ahmad AL, Hameed BH. Enhancement of basic dye adsorption uptake from aqueous solutions using chemically modified oil palm shell activated carbon. Colloids Surfaces a Physicochem Eng Asp. 2008;318(1–3):88–96. https://doi.org/10.1016/j.colsurfa.2007.12.018

[17]   Low LW, Teng TT, Ahmad A, Morad N, Wong YS. A novel pretreatment method of lignocellulosic material as adsorbent and kinetic study of dye waste adsorption. Water, Air, Soil Pollut. 2011;218(1):293–306. https://doi.org/10.1007/s11270-010-0642-3

[18]   Senthilkumaar S, Varadarajan PR, Porkodi K, Subbhuraam C V. Adsorption of methylene blue onto jute fiber carbon: kinetics and equilibrium studies. J Colloid Interface Sci. 2005;284(1):78–82. https://doi.org/10.1016/j.jcis.2004.09.027

[19]   Jawad AH, Rashid RA, Mahmuod RMA, Ishak MAM, Kasim NN, Ismail K. Adsorption of methylene blue onto coconut (Cocos nucifera) leaf: optimization, isotherm and kinetic studies. Desalin Water Treat. 2016;57(19):8839–53. https://doi.org/10.1080/19443994.2015.1026282

[20]   Davarnejad R, Pishdad R, Sepahvand S. Dye adsorption ON the blends of saffron petals powder with activated carbon: Response surface methodology. Int J Eng. 2018;31(12):2001–8. https://doi: 10.5829/ije.2018.31.12c.02

[21]   Masomi M, Ghoreyshi AA, Najafpour GD, Mohamed AR. Adsorption of phenolic compounds onto the activated carbon synthesized from pulp and paper mill sludge: Equilibrium isotherm, kinetics, thermodynamics and mechanism studies. Int J Eng. 2014;27(10):1485-1494. https://doi: 10.5829/idosi.ije.2014.27.10a.01

[22]   Hayashi J, Kazehaya A, Muroyama K, Watkinson AP. Preparation of activated carbon from lignin by chemical activation. Carbon N Y. 2000;38(13):1873–8. https://doi.org/10.1016/S0008-6223(00)00027-0

[23]   Li W, Yang K, Peng J, Zhang L, Guo S, Xia H. Effects of carbonization temperatures on characteristics of porosity in coconut shell chars and activated carbons derived from carbonized coconut shell chars. Ind Crops Prod. 2008;28(2):190–8. https://doi.org/10.1016/j.indcrop.2008.02.012

[24]   Rosas JM, Berenguer R, Valero-Romero MJ, Rodríguez-Mirasol J, Cordero T. Preparation of different carbon materials by thermochemical conversion of lignin. Front Mater. 2014; 1:29. https://doi.org/10.3389/fmats.2014.00029

[25]   Meng L-Y, Ma M-G, Ji X-X. Preparation of lignin-based carbon materials and its application as a sorbent. Materials (Basel). 2019;12(7):1111. https://doi.org/10.3390/ma12071111

[26]   Khezami L, Chetouani A, Taouk B, Capart R. Production and characterisation of activated carbon from wood components in powder: Cellulose, lignin, xylan. Powder Technol. 2005;157(1–3):48–56. https://doi.org/10.1016/j.powtec.2005.05.009

[27]   Smook GA. Handbook for pulp & paper technologists. A. Wilde; 2002. eBook ISBN: 0969462859

[28]   Mussatto SI, Fernandes M, Roberto IC. Lignin recovery from brewer's spent grain black liquor. Carbohydr Polym. 2007;70(2):218–23. https://doi.org/10.1016/j.carbpol.2007.03.021

[29]   Kim J-M, Song I-S, Cho D-H, Hong I-P. Effect of carbonization temperature and chemical pre-treatment on the thermal change and fiber morphology of kenaf-based carbon fibers. Carbon Lett. 2011;12(3):131–7. https://doi.org/10.5714/CL.2011.12.3.131

[30]   Harding AW, Foley NJ, Norman PR, Francis DC, Thomas KM. Diffusion barriers in the kinetics of water vapor adsorption/desorption on activated carbons. Langmuir. 1998;14(14):3858–64. https://doi.org/10.1021/la971317o

[31]   Cho D, Kim JM, Song IS, Hong I. Effect of alkali pre-treatment of jute on the formation of jute-based carbon fibers. Mater Lett. 2011;65(10):1492–4. https://doi.org/10.1016/j.matlet.2011.02.050

[32]   Phan NH, Rio S, Faur C, Le Coq L, Le Cloirec P, Nguyen TH. Production of fibrous activated carbons from natural cellulose (jute, coconut) fibers for water treatment applications. Carbon N Y. 2006;44(12):2569–77. https://doi.org/10.1016/j.carbon.2006.05.048

[33]   Li J, Zhang H, Tang X, Lu H. Adsorptive desulfurization of dibenzothiophene over lignin-derived biochar by one-step modification with potassium hydrogen phthalate. RSC Adv. 2016;6(102):100352–60. https://doi.org/10.1039/C6RA20220A

[34]   Gao Y, Yue Q, Gao B, Sun Y, Wang W, Li Q, et al. Preparation of high surface area-activated carbon from lignin of papermaking black liquor by KOH activation for Ni (II) adsorption. Chem Eng J. 2013; 217:345–53. https://doi.org/10.1016/j.cej.2012.09.038

[35]   Liao Z, Zhu Y-H, Sun G-T, Qiu L, Zhu M-Q. Micromorphology control of the lignin-based activated carbon and the study on the pyrolysis and adsorption kinetics. Ind Crops Prod. 2022; 175:114266. https://doi.org/10.1016/j.indcrop.2021.114266

[36]   Williams PT, Reed AR. Development of activated carbon pore structure via physical and chemical activation of biomass fibre waste. Biomass and Bioenergy. 2006;30(2):144–52. https://doi.org/10.1016/j.biombioe.2005.11.006

[37]   Somsesta N, Sricharoenchaikul V, Aht-Ong D. Adsorption removal of methylene blue onto activated carbon/cellulose biocomposite films: equilibrium and kinetic studies. Mater Chem Phys. 2020; 240:122221. https://doi.org/10.1016/j.matchemphys.2019.122221

[38]   Fengel D, Wegener G, Greune A. Studies on the delignification of spruce wood by organosolv pulping using SEM-EDXA and TEM. Wood Sci Technol. 1989;23(2):123–30. https://doi.org/10.1007/BF00350934

[39]   Brazil TR, Gonçalves M, Junior MSO, Rezende MC. Sustainable process to produce activated carbon from Kraft lignin impregnated with H3PO4 using microwave pyrolysis. Biomass and Bioenergy. 2022; 156:106333. https://doi.org/10.1016/j.biombioe.2021.106333

[40]   Kim D, Cheon J, Kim J, Hwang D, Hong I, Kwon OH, et al. Extraction and characterization of lignin from black liquor and preparation of biomass-based activated carbon there-from. Carbon Lett. 2017; 22:81–8. https://doi.org/10.5714/CL.2017.22.081

[41]   Higuchi T. Biochemistry of wood components: biosynthesis and microbial degradation of lignin. Wood Res Bull Wood Res Inst Kyoto Univ. 2002; 89:43–51. http://hdl.handle.net/2433/53120

[42] Fu K, Yue Q, Gao B, Sun Y, Zhu L. Preparation, characterization and application of lignin-based activated carbon from black liquor lignin by steam activation. Chem Eng J. 2013; 228:1074–82. https://doi.org/10.1016/j.cej.2013.05.028

[43] Ahrland S, Bagnall KW, Brown D. The chemistry of the actinides: comprehensive inorganic chemistry. Elsevier; 2016. eBook ISBN: 9781483159348

[44] Fierro V, Torné-Fernández V, Celzard A. Kraft lignin as a precursor for microporous activated carbons prepared by impregnation with ortho-phosphoric acid: Synthesis and textural characterisation. Microporous mesoporous Mater. 2006;92(1–3):243–50. https://doi.org/10.1016/j.micromeso.2006.01.013

[45] Gonzalez-Serrano E, Cordero T, Rodriguez-Mirasol J, Cotoruelo L, Rodriguez JJ. Removal of water pollutants with activated carbons prepared from H3PO4 activation of lignin from kraft black liquors. Water Res. 2004;38(13):3043–50. https://doi.org/10.1016/j.watres.2004.04.048

[46] Zhang J, Yu L, Wang Z, Tian Y, Qu Y, Wang Y, et al. Spherical microporous/mesoporous activated carbon from pulping black liquor. J Chem Technol Biotechnol. 2011;86(9):1177–83. https://doi.org/10.1002/jctb.2627

[47] Jawad AH, Rashid RA, Ishak MAM, Wilson LD. Adsorption of methylene blue onto activated carbon developed from biomass waste by H2SO4 activation: kinetic, equilibrium and thermodynamic studies. Desalin Water Treat. 2016;57(52):25194–206. https://doi.org/10.1080/19443994.2016.1144534

[48] de Castro CS, Viau LN, Andrade JT, Mendonça TAP, Gonçalves M. Mesoporous activated carbon from polyethyleneterephthalate (PET) waste: pollutant adsorption in aqueous solution. New J Chem. 2018;42(17):14612–9. https://doi.org/10.1039/C8NJ02715C

[49] Hameed BH, Tan IAW, Ahmad AL. Adsorption isotherm, kinetic modeling and mechanism of 2, 4, 6-trichlorophenol on coconut husk-based activated carbon. Chem Eng J. 2008;144(2):235–44. https://doi.org/10.1016/j.cej.2008.01.028

[50] Fytianos K, Voudrias E, Kokkalis E. Sorption–desorption behaviour of 2, 4-dichlorophenol by marine sediments. Chemosphere. 2000;40(1):3–6. https://doi.org/10.1016/S0045-6535(99)00214-3

[51] Özacar M, Şengil İA. Application of kinetic models to the sorption of disperse dyes onto alunite. Colloids Surfaces a Physicochem Eng Asp. 2004;242(1–3):105–13. https://doi.org/10.1016/j.colsurfa.2004.03.029

[52] Basaleh AA, Al-Malack MH, Saleh TA. Methylene Blue removal using polyamide-vermiculite nanocomposites: Kinetics, equilibrium and thermodynamic study. J Environ Chem Eng. 2019;7(3):103107. https://doi.org/10.1016/j.jece.2019.103107

[53] Ma H, Li J-B, Liu W-W, Miao M, Cheng B-J, Zhu S-W. Novel synthesis of a versatile magnetic adsorbent derived from corncob for dye removal. Bioresour Technol. 2015; 190:13–20. https://doi.org/10.1016/j.biortech.2015.04.048

[54] El Messaoudi N, El Khomri M, Bentahar S, Dbik A, Lacherai A, Bakiz B. Evaluation of performance of chemically treated date stones: application for the removal of cationic dyes from aqueous solutions. J Taiwan Inst Chem Eng. 2016; 67:244–53. https://doi.org/10.1016/j.jtice.2016.07.024

[55] Ji Y, Xu F, Wei W, Gao H, Zhang K, Zhang G, et al. Efficient and fast adsorption of methylene blue dye onto a nanosheet MFI zeolite. J Solid State Chem. 2021; 295:121917. https://doi.org/10.1016/j.jssc.2020.121917